Calculation of the Frequency Characteristics of Microstrips Discontinuities on Non-Diagonal Anisotropic Substrates Using FDTD

S. M. Chehrehrazi and A. R. Baghai-Wadji*
Department of Applied Electronics, IAEE 359/2, Vienna University of Technology
Gußhausstraße 27-29, A-1040 Vienna, Austria
* Motorola, Inc., 8201 E. McDowell Rd., M.D. H1562, Scottsdale, AZ 85252, USA and,
Arizona State University, Department of Mathematics, Tempe, AZ 85287, USA

Abstract—**This paper describes modifications of the conventional finite-difference time-domain (FDTD) method to the full-wave analysis of frequency-dependent characteristics of microstrips discontinuities on non-diagonal anisotropic substrates. The application of the conventional FDTD is limited to materials with diagonal-anisotropic material matrices. In this paper it is shown that this restriction can be removed: First, steps for obtaining the FDTD equations for the analysis of microstrips discontinuities on substrates with fully anisotropic permittivity matrices are derived. Then, using the Fourier transform of the computed results in the time-domain, the scattering parameters as functions of the frequency are calculated for several examples.**

I. Introduction

The finite-difference time-domain (FDTD) method was first proposed by Yee [1]. It is formulated by using Maxwell's curl equations over a finite volume and approximating the involved derivatives with centered difference technique. Analysis of the discontinuities is of great importance since more complicated circuits can be realized by interconnecting microstrip lines with these discontinuities. The FDTD method promises a great flexibility in handling a variety of microstrip discontinuities [2], [3], [5]. However, the results published so far are limited to substrates that are either isotropic or have diagonal permittivity matrices. Many materials used as substrates for integrated microwave circuits or printed-circuit antennas exhibit dielectric anisotropy which either occurs naturally in the material or is introduced during the manufacturing process. The development of accurate methods for the design of these circuits requires a precise knowledge of the substrate material dielectric constants. The variations in the values of the substrate material relative dielectric constants introduce errors in integrated circuit design and reduce its reproducibility. For these reasons and because in certain applications anisotropy serves to improve performance, it must be fully and accurately accounted for. In this paper, we outline the steps to obtain the FDTD equations for the analysis of microstips discontinuities on non-diagonal anisotropic substrates. We use these equations to obtain the scattering parameters for microstrip discontinuities on Quartz as the substrate material.

Manuscript received September 23, 1996.
S. M. Chehrehrazi, e-mail: mchehre@rs1.iaee.tuwien.ac.at,
A. R. Baghai Wadji is on leave of absence from Vienna University of Technology, IAEE 359/2, Gußhausstraße 27-29, A-1040 Vienna, Austria, e-mail: p0141c@email.mot.com

II. Problem Formulation

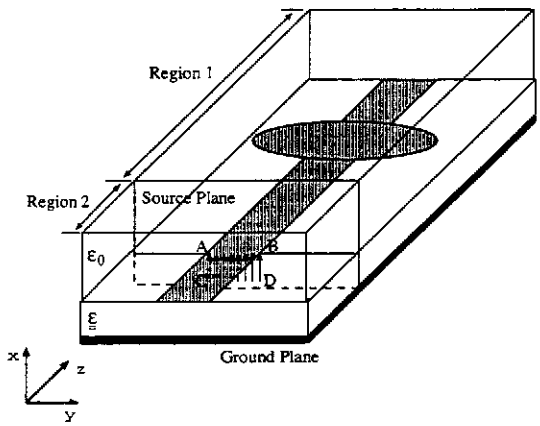

Fig. 1. Computational domain

The computational domain and the generalized microstrip discontinuity under investigation is shown in Fig. 1 (a more complete configuration would describe an N-port microstrip instead of a two-port). The strip and the bottom plane are perfect conductors ($\sigma \to \infty$) and the substrate is characterized by the constant permittivity matrix $\underline{\underline{\varepsilon}}$

$$\underline{\underline{\varepsilon}} = \varepsilon_0 \begin{bmatrix} \varepsilon_{xx} & \varepsilon_{xy} & \varepsilon_{xz} \\ \varepsilon_{yx} & \varepsilon_{yy} & \varepsilon_{yz} \\ \varepsilon_{zx} & \varepsilon_{zy} & \varepsilon_{zz} \end{bmatrix}. \tag{1}$$

Furthermore, a uniaxial permeability matrix is assumed.

$$\underline{\underline{\mu}} = \mu_0 \begin{bmatrix} \mu_{xx} & 0 & 0 \\ 0 & \mu_{yy} & 0 \\ 0 & 0 & \mu_{zz} \end{bmatrix} \tag{2}$$

The structure is taken to be in an open environment, that is, above the dielectric and the metal strip surface, free space is assumed to extend to infinity. The substrate-ground plane also extends uniformly into infinity. With

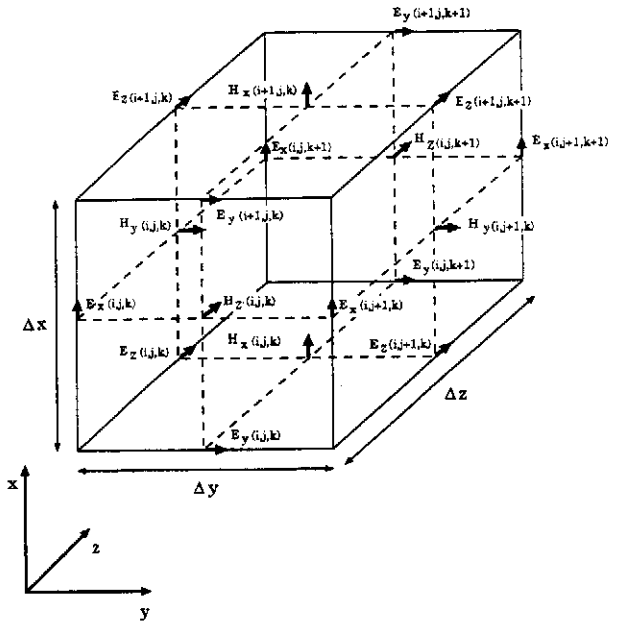

Fig. 2. Yee's placement of the fieldcomponents in the FDTD unit cell.

these assumptions, Maxwell's curl equations for source free regions read

$$\vec{\nabla} \times \mathbf{E} = -\underline{\underline{\mu}} \frac{\partial \mathbf{H}}{\partial t}, \tag{3a}$$

$$\vec{\nabla} \times \mathbf{H} = \underline{\underline{\varepsilon}} \frac{\partial \mathbf{E}}{\partial t}. \tag{3b}$$

In order to find an approximate solution to this set of equations, the problem is discretized over a finite three dimensional computational domain with appropriate boundary conditions enforced on the conductors, dielectric-air interface, and the mesh walls.

A. Time-Domain Finite Difference Equations

The centered difference scheme is used to approximate both the time and the space first-order partial derivatives to obtain discrete approximations to the continuous partial equations (3). To simulate the wave propagation in FDTD algorithm, the six field locations are considered to be interleaved in space as shown in Fig. 2, which is a drawing of the FDTD unit cell arranged by Yee [1]. The entire computational domain is obtained by stacking these rectangular cubes into a larger rectangular volume. The advantages of this field arrangement are that centered differences are obtained in the calculation of each field component and that continuity of tangential field components is automatically satisfied. In this algorithm, not only the placement of **E** and **H** nodes are off in space by half a space step, but the time instants when the **E** or **H** fields are calculated are also off by half a time step. We will use the following notation for our discretization: assuming the function $F(x, y, z, t)$ is evaluated at the node $(i\Delta x,\ j\Delta y,\ k\Delta z, n\Delta t)$, this function can be written as $F^n(i, j, k) = F(i\Delta x, j\Delta y, k\Delta z, n\Delta t)$, where (i, j, k) represents numbers of the nodes in computational domain in x, y and z directions and the superscript n indicates the time step.

H- *Field Equations:*

Using this arrangement for the field components and the centered difference scheme, an approximation to (3a) can be obtained at the node $(i\Delta x,\ j\Delta y,\ k\Delta z, (n+\frac{1}{2})\Delta t)$:

$$H_x{}^{n+\frac{1}{2}}(i,j,k) = H_x{}^{n-\frac{1}{2}}(i,j,k) - \frac{\Delta t}{\mu_0 \mu_{xx}} \left[\frac{E_z{}^n(i,j+1,k) - E_z{}^n(i,j,k)}{\Delta y} - \frac{E_y{}^n(i,j,k+1) - E_y{}^n(i,j,k)}{\Delta z} \right] \tag{4a}$$

$$H_y{}^{n+\frac{1}{2}}(i,j,k) = H_y{}^{n-\frac{1}{2}}(i,j,k) - \frac{\Delta t}{\mu_0 \mu_{yy}} \left[\frac{E_x{}^n(i,j,k+1) - E_x{}^n(i,j,k)}{\Delta z} - \frac{E_z{}^n(i+1,j,k) - E_z{}^n(i,j,k)}{\Delta x} \right] \tag{4b}$$

$$H_z{}^{n+\frac{1}{2}}(i,j,k) = H_z{}^{n-\frac{1}{2}}(i,j,k) - \frac{\Delta t}{\mu_0 \mu_{zz}} \left[\frac{E_y{}^n(i+1,j,k) - E_y{}^n(i,j,k)}{\Delta x} - \frac{E_x{}^n(i,j+1,k) - E_x{}^n(i,j,k)}{\Delta y} \right] \tag{4c}$$

E- *Field Equations:*

The existence of off-diagonal elements in the permittivity matrix leads to the coupling between the time derivatives of the electric field components. Separating (3b) into scalar components, we obtain the following equation in matrix form for electric field components at the time step $n+1$:

$$\begin{bmatrix} E_x \big|_{i,j,k}^{n+1} \\ E_y \big|_{i,j,k}^{n+1} \\ E_z \big|_{i,j,k}^{n+1} \end{bmatrix} = \begin{bmatrix} E_x \big|_{i,j,k}^{n} \\ E_y \big|_{i,j,k}^{n} \\ E_z \big|_{i,j,k}^{n} \end{bmatrix} + \frac{\Delta t}{\varepsilon_0 Det} \underline{\underline{M}} \begin{bmatrix} \frac{\partial H_z}{\partial y} \big|_{i,j,k}^{n+\frac{1}{2}} - \frac{\partial H_y}{\partial z} \big|_{i,j,k}^{n+\frac{1}{2}} \\ \frac{\partial H_x}{\partial z} \big|_{i,j,k}^{n+\frac{1}{2}} - \frac{\partial H_z}{\partial x} \big|_{i,j,k}^{n+\frac{1}{2}} \\ \frac{\partial H_y}{\partial x} \big|_{i,j,k}^{n+\frac{1}{2}} - \frac{\partial H_x}{\partial y} \big|_{i,j,k}^{n+\frac{1}{2}} \end{bmatrix}. \tag{5}$$

$\underline{\underline{M}}$ and Det denote the adjoint and the determinant of $\underline{\underline{\varepsilon}}$, respectively. We now examine this result. The expression

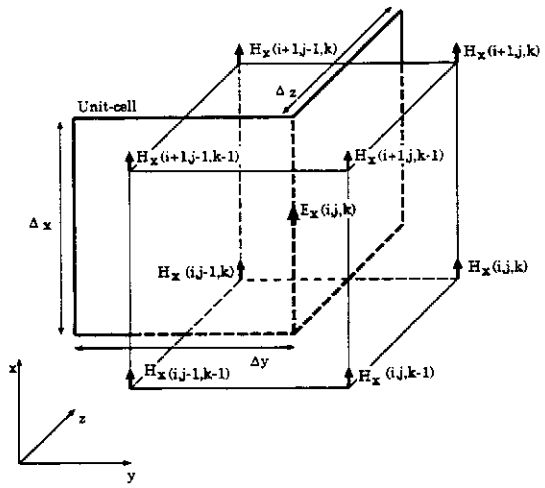

Fig. 3. On the approximation of $\frac{\partial H_x}{\partial z}\Big|_{i,j,k}^{n+\frac{1}{2}}$.

of the electric field component E_x is

$$E_x\Big|_{i,j,k}^{n+1} = E_x\Big|_{i,j,k}^{n} + \frac{\Delta t}{\varepsilon_0 Det} \cdot \left\{ m_{xx}\left(\frac{\partial H_z}{\partial y}\Big|_{i,j,k}^{n+\frac{1}{2}} - \frac{\partial H_y}{\partial z}\Big|_{i,j,k}^{n+\frac{1}{2}}\right) + m_{xy}\left(\frac{\partial H_x}{\partial z}\Big|_{i,j,k}^{n+\frac{1}{2}} - \frac{\partial H_z}{\partial x}\Big|_{i,j,k}^{n+\frac{1}{2}}\right) + m_{xz}\left(\frac{\partial H_y}{\partial x}\Big|_{i,j,k}^{n+\frac{1}{2}} - \frac{\partial H_x}{\partial y}\Big|_{i,j,k}^{n+\frac{1}{2}}\right)\right\}. \quad (6)$$

It is readily seen that this equation reduces to the corresponding standard FDTD equation, if the off-diagonal terms of $\underline{\underline{\varepsilon}}$ are zero. ($m_{xy} = m_{xz} = 0$.) Note that $m_{xx} \neq 0$ is guaranteed for positive definite dielectric matrices. The derivatives $\frac{\partial H_z}{\partial y}\Big|_{i,j,k}^{n+\frac{1}{2}}$ and $\frac{\partial H_y}{\partial z}\Big|_{i,j,k}^{n+\frac{1}{2}}$ are obtained in the usual manner directly from the FDTD grid. In order to calculate the remaining derivatives, $\frac{\partial H_x}{\partial z}\Big|_{i,j,k}^{n+\frac{1}{2}}$, $\frac{\partial H_z}{\partial x}\Big|_{i,j,k}^{n+\frac{1}{2}}$, $\frac{\partial H_y}{\partial x}\Big|_{i,j,k}^{n+\frac{1}{2}}$ and $\frac{\partial H_x}{\partial y}\Big|_{i,j,k}^{n+\frac{1}{2}}$ an approximate interpolation technique has been proposed.
Fig. 3 shows the position of E_x in each unit cell along with the surrounding H_x field components of this electric field component. For $\frac{\partial H_x}{\partial z}\Big|_{i,j,k}^{n+\frac{1}{2}}$ we obtain

$$\frac{\partial H_x}{\partial z}\Big|_{i,j,k}^{n+\frac{1}{2}} = \frac{1}{4\Delta z} \cdot \Big\{ {H_x}^{n+\frac{1}{2}}(i+1,j,k) + {H_x}^{n+\frac{1}{2}}(i,j,k) + {H_x}^{n+\frac{1}{2}}(i+1,j-1,k) + {H_x}^{n+\frac{1}{2}}(i,j-1,k) - {H_x}^{n+\frac{1}{2}}(i+1,j,k-1) - {H_x}^{n+\frac{1}{2}}(i,j,k-1) - {H_x}^{n+\frac{1}{2}}(i+1,j-1,k-1) - {H_x}^{n+\frac{1}{2}}(i,j-1,k-1)\Big\}. \quad (7)$$

Considering the Fig. 4, we obtain the following result for $\frac{\partial H_z}{\partial x}\Big|_{i,j,k}^{n+\frac{1}{2}}$:

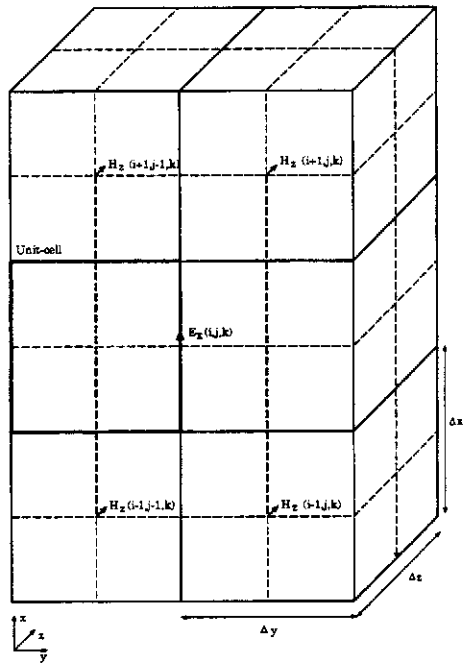

Fig. 4. On the approximation of $\frac{\partial H_z}{\partial x}\Big|_{i,j,k}^{n+\frac{1}{2}}$.

$$\frac{\partial H_z}{\partial x}\Big|_{i,j,k}^{n+\frac{1}{2}} = \frac{1}{4\Delta x} \cdot \Big\{ {H_z}^{n+\frac{1}{2}}(i+1,j,k) + {H_z}^{n+\frac{1}{2}}(i+1,j-1,k) - {H_z}^{n+\frac{1}{2}}(i-1,j,k) - {H_z}^{n+\frac{1}{2}}(i-1,j-1,k)\Big\}. \quad (8)$$

$\frac{\partial H_y}{\partial x}\Big|_{i,j,k}^{n+\frac{1}{2}}$ is obtained through our interpolation as follow:

$$\frac{\partial H_y}{\partial x}\Big|_{i,j,k}^{n+\frac{1}{2}} = \frac{1}{4\Delta x} \cdot \Big\{ {H_y}^{n+\frac{1}{2}}(i+1,j,k) + {H_y}^{n+\frac{1}{2}}(i+1,j,k-1) - {H_y}^{n+\frac{1}{2}}(i-1,j,k) - {H_y}^{n+\frac{1}{2}}(i-1,j,k-1)\Big\}. \quad (9)$$

$\frac{\partial H_x}{\partial y}\Big|_{i,j,k}^{n+\frac{1}{2}}$ can be obtained in the same manner as $\frac{\partial H_x}{\partial z}\Big|_{i,j,k}^{n+\frac{1}{2}}$. To this end we construct the differences of the magnetic field components in the neighborhood of E_x in y direction.
Similar expressions can easily be obtained for E_y and E_z. The maximum time step that may be used is limited by the stability condition of the finite difference equations,

$$\Delta t \leq \frac{1}{c_{max}}\left(\frac{1}{\Delta x^2} + \frac{1}{\Delta y^2} + \frac{1}{\Delta z^2}\right)^{-1/2} \quad (10)$$

where c_{max} is the maximum velocity of light in the computational domain. In our calculations c_{max} is the velocity of light in free space because the computational domain is partially filled with air.

B. Dielectric-Air Interface Conditions

The above finite difference equations for **H** and **E** Field components are derived in the uniform dielectric region of

the computational domain (Fig. 1) and therefore cannot be applied to the nodal points located on the dielectric-air interface or on the boundary walls of the mesh. All these points require special treatment. The field components which lie on the dielectric-air interface are the tangential components of $\mathbf{E}$ (E_y and E_z) and the vertical component of $\mathbf{H}$ (H_x). In calculating H_x, (4a) can still be used because the value of permeability does not change across the interface, and the E_y and E_z components used for the calculation of H_x are the tangential components with respect to the interface and are thus continuous across the boundary. To calculate E_y and E_z, however, a special finite difference formulation must be derived from the field continuity conditions across the boundary. The expression for E_y within the assumed dielectric is

$$\left(\frac{\partial E_y}{\partial t}\right)_{sub} = \frac{1}{\epsilon_0 Det} \cdot \left\{ m_{xy}\left(\frac{\partial H_z}{\partial y} - \frac{\partial H_y}{\partial z}\right) + m_{yy}\left(\frac{\partial H_x}{\partial z} - \frac{\partial H_z}{\partial x}\right) + m_{yz}\left(\frac{\partial H_y}{\partial x} - \frac{\partial H_x}{\partial y}\right)\right\}, \quad (11)$$

while the expression for E_y in free space is

$$\left(\frac{\partial E_y}{\partial t}\right)_{air} = \frac{1}{\epsilon_0}\left\{\frac{\partial H_x}{\partial z} - \frac{\partial H_z}{\partial x}\right\}. \quad (12)$$

For the calculation of E_y on the interface, we add these expressions and apply the continuity condition

$$\left(\frac{\partial E_y}{\partial t}\right)_{sub}\Big|_{x=0^-} = \left(\frac{\partial E_y}{\partial t}\right)_{air}\Big|_{x=0^+} = \left(\frac{\partial E_y}{\partial t}\right)_{inter} \quad (13)$$

across the interface. As numerical calculations in [2] and [7] have shown, we can assume that $\partial H_z/\partial x$ and $\partial H_y/\partial x$ are continuous. Therefore, we obtain an expression for the calculation of E_y on the interface

$$\left(\frac{\partial E_y}{\partial t}\right)_{inter} = \frac{1}{2\epsilon_0 Det} \cdot \left\{ m_{xy}\left(\frac{\partial H_z}{\partial y} - \frac{\partial H_y}{\partial z}\right) + (m_{yy} + Det)\left(\frac{\partial H_x}{\partial z} - \frac{\partial H_z}{\partial x}\right) + m_{yz}\left(\frac{\partial H_y}{\partial x} - \frac{\partial H_x}{\partial y}\right)\right\}. \quad (14)$$

A similar expression can be obtained for E_z. E_y and E_z vanish on a metal strip because of the assumption of perfectly conducting surface.

C. Absorbing Boundary Conditions

Due to the finite capabilities of the computers used to implement the finite-difference equations, the mesh must be truncated in x, y and z directions. The difference equations cannot be used to evaluate the field components tangential to outer boundaries since they would require the values of field components outside of the mesh. The ground plane is a perfect conductor and the tangential electric field is forced to be zero on it. The tangential electric field components on the remaining five mesh walls must be specified in such a way that outgoing waves are not reflected using the absorbing boundary conditions (ABC's). The Mur's first absorbing boundary condition is utilized for the calculation of microstrip discontinuities in this work [4]. For a wall normal to the z-axis Mur's first ABC's may be written in the form

$$\left(\frac{\partial}{\partial z} - \frac{1}{v}\frac{\partial}{\partial t}\right)\mathbf{E}_{tan} = 0. \quad (15)$$

This equation can be discretized using field components on or just inside the mesh wall, yielding an explicit finite difference equation

$$E_0^{n+1} = E_1^n + \frac{v\Delta t - \Delta z}{v\Delta t + \Delta z}\left(E_1^{n+1} - E_0^n\right), \quad (16)$$

where E_0 stands for the tangential components of $\mathbf{E}$ on the mesh wall and E_1 represent the tangential components of $\mathbf{E}$ one node inside of the mesh wall. Similar expressions can be obtained for the remaining ABC's by using the corresponding normal directions for each wall. It should be noted that the normal incidence assumption is not valid for the fringing fields which are propagating tangential to the walls; therefore the sidewalls should be far enough away that the fringing fields become negligible at the walls.

D. Excitation Pulse and Source Modeling

In order to simulate a voltage source excitation it is necessary to impose the vertical electric field E_x in a rectangular region ABCD underneath the input of the microstrip in the source plane $k = k_S$ (see Fig. 1). The launched wave has unit amplitude and is Gaussian in time

$$E_{xGen} = \begin{cases} e^{-(t-t_0)^2/T^2} & : \ (x,y) \in \text{ABCD} \\ 0 & : \ \text{elsewhere.} \end{cases} \quad (17)$$

The source plane being parallel to the (x,y) plane is located several nodes away from the boundary inside the computational domain (Fig. 1). This plane divides the computational domain into region 1, containing the microstrip discontinuity, and region 2, containing the absorbing boundary. For field wave ${E_x}^{n+1}(i,j,k_S)$ on the source plane we obtain

$${E_x}^{n+1}(i,j,k_S) = E_x\Big|^n_{i,j,k_s} + E_{xGen}\Big|^n \quad (18)$$

where $E_x\Big|^n_{i,j,k_s}$ represents the term at the left-hand side of Eq.(6) evaluated at the time step n. On the source plane, no special treatment is applied to the remaining EM field components. They are calculated from (4) and (5). With this modeling technique for the excitation [6], the dc source distortions reported in [2] and [5] are not apparent.

III. Numerical Results

In order to determine the scattering parameters of microstrips discontinuities by means of FDTD, Fourier transform of incident and reflected transient waveforms must be used. We assume reference planes (i.e. $T-T$ in Figs. (5) and (6) in the sides of discontinuities and record the vertical electric field one node underneath the center of microstrip of each reference plane at every time step. The scattering parameters S_{jk} may then be obtained by Fourier transform of these transient waveforms as

$$S_{jk}(f) = \frac{\mathcal{FT}[V_j(t)]}{\mathcal{FT}[V_k(t)]}. \tag{19}$$

The reference planes are chosen far enough from the discontinuities to eliminate evanescent waves.

Examples

In this work, two types of symmetric microstrip discontinuities on Quartz substrate with permittivity matrix

$$\underline{\underline{\varepsilon}} = \varepsilon_0 \begin{bmatrix} 4.53 & -0.34 & -0.24 \\ -0.34 & 4.30 & 0.13 \\ -0.24 & 0.13 & 4.75 \end{bmatrix} \tag{20}$$

and the permeabilities $\mu_{xx} = \mu_{yy} = \mu_{zz} = 1$ have been calculated. In our calculations the parameters of the structure and the mesh have been selected as follows.
thickness of the substrate: $h = 0.5\ mm$
width of the metal strip: $w = 1.0\ mm$
mesh size: $20 \times 80 \times 100$
$\Delta x = \Delta y = \Delta z = 0.1\ mm$
$\Delta t = 0.120\ ps$.

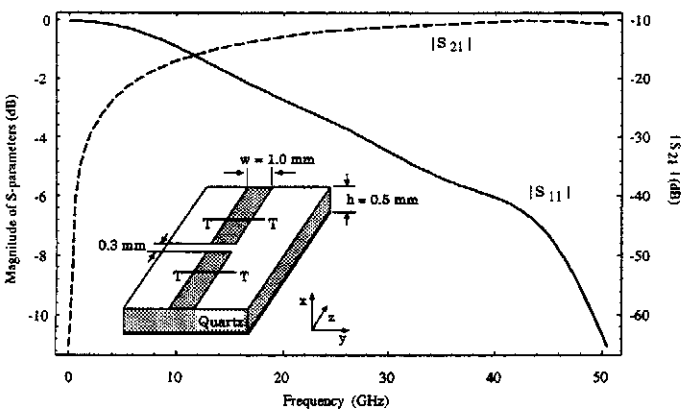

Fig. 5. S_{11} and S_{21} parameters of the microstrip gap.

IV. Conclusion

We have extended the conventional FDTD method to include non-diagonal permittivity matrix for calculating the frequency characteristics of microstrips discontinuities on fully anisotropic materials over a large frequency range.

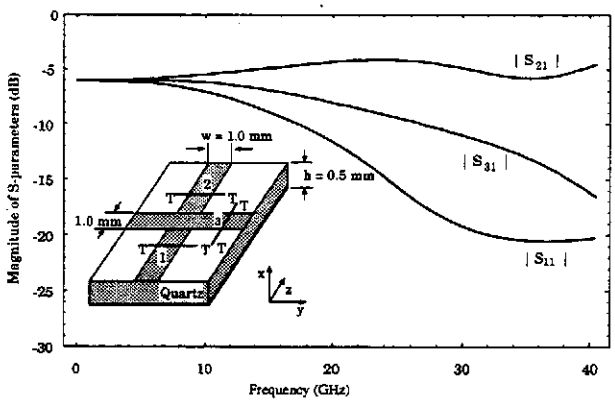

Fig. 6. S-parameters of the microstrip cross-junction.

References

[1] K.S. Yee, "Numerical solution of initial boundary value problems involving maxwell's equations in isotropic media," *IEEE Trans. Antennas Propagat.*, vol. Ap-14, pp. 302-307, 1966.

[2] X. Zhang, and K. K. Mei "Time-domain finite difference approach to the calculation of the frequency-dependent characteristics of microstrip discontinuities," *IEEE Trans. Microwave Theory Tech.*, vol. MTT-36, pp. 1775-1787, 1988.

[3] D. H. Choi and W. J. R. Hoefer "The finite-difference-time-domain method and its application to eigenvalue problems," *IEEE Trans. Microwave Theory Tech.*, vol. MTT-34, pp. 104-109, 1986.

[4] G. Mur, "Absorbing boundary conditions for the finite difference approximation of the time domain electromagnetic field equations," *IEEE Trans. Electromagn. Compat.*, vol. EMC-23, pp. 377-382, 1981.

[5] D. M. Sheen, M. A. Sami,M. D. Abouzahra and J. Au Kong, "Application of the three-dimensional finite-difference time-domain method to the analysis of planar microstrip circuits," *IEEE Trans. Microwave Theory Tech.*, vol. MTT-38, pp. 849-856, 1990.

[6] A. P. Zhao, A. V. Räisänen and S. R. Cvetkovic, "A fast and efficient FDTD algorithm for the analysis of planar microstrip discontinuities by using a simple source excitation scheme," *IEEE Microwave and Guided Wave Lett.*, vol. 5, pp. 341-343, no. 10, 1995.

[7] A. Reineix and B. Jecko, "Analysis of microstrip patch antennas using finite difference time domain method," *IEEE Trans. Antennas and Propagation*, vol. AP-37, pp. 1361-1369, 1989.